IEEE Access
Multidisciplinary | Rapid Review | Open Access Journal

Received March 17, 2019, accepted April 29, 2019, date of publication May 22, 2019, date of current version October 17, 2019.

Digital Object Identifier 10.1109/ACCESS.2019.2918384

Distributed Adaptive Control for UAV Formation With Input Saturation and Actuator Fault

ZHONG ZHENG[1], MOSHU QIAN[1,2], PENG LI[3], AND HUI YI[1]

[1]College of Electrical Engineering and Control Science, Nanjing Tech University, Nanjing 210000, China
[2]State Key Laboratory of Mechanics and Control of Mechanical Structures, Nanjing University of Aeronautics and Astronautics, Nanjing 210016, China
[3]College of Information Engineering, Xiangtan University, Xiangtan 411105, China

Corresponding author: Zhong Zheng (zhengzhong8610@126.com)

This work was supported in part by the National project funding for Key R&D programs under Grant 2018YFC0808500, in part by the Postdoctoral Research Foundation of Jiangsu Province under Grant 1701140B, in part by the GF Research and Development Project of Nanjing Tech University under Grant 201709, in part by the Natural Science Foundation of the Jiangsu Higher Education Institutions of China under Grant 18KJB413004, and in part by the Key Point Research And Invention Program in Hunan Province of China under Grant 2018GK2014.

ABSTRACT The distributed adaptive tracking control schemes are addressed to deal with the formation control problem of multiple unmanned aerial vehicles subject to input saturation, actuator fault, and external disturbance. First, a novel adaptive backstepping control approach associated with a command filter is presented to settle the model uncertainty and input saturation problems. Second, a robust fault-tolerant controller is introduced to tackle the case with external disturbance, actuator fault, and model uncertainty by estimating the upper bounds of the faults and external disturbances. In addition, the proposed controllers enable the asymptotical stability of the closed-loop system in case of undirected interaction graph. Finally, the numerical simulations demonstrate that the proposed approaches are effective for the unmanned aircraft vehicle (UAV) formation system with various constraints.

INDEX TERMS UAV formation, backstepping control, input saturation, actuator fault, asymptotical stability.

I. INTRODUCTION

Formation control for multiple unmanned aircraft vehicles (UAVs) has attracted the burgeoning interest during the past several years [1]–[4], since it promises great potentials in both civilian and military applications, such as surveillance, reconnaissance, rescue missions, fire monitoring [5]–[7], to name a few. Some of these tasks may be parlous and not suitable for human pilots. To this end, it is appropriate to complete the tasks above using autonomous UAVs in a formation. From a practical point of view, the design of efficient control approach for the UAVs is an undoubtedly central issue to bring about trajectory tracking in the formation.

The formation control for UAVs indicates designing centralized or distributed control algorithms to drive the UAVs to the desired formation while maintaining the expected relative position and common velocity. The distributed control strategy for UAV formation, which makes use of the local information of the neighbors, becomes one choice to accomplish intricate formation tasks with high control accuracy, robustness and environmental adaption. Generally, there are three control approaches in this field, namely behavioral, leader-following, and virtual structure based formation control [8]. Correspondingly, several formation control algorithms for UAVs have been presented, including model predictive control scheme [9], [10], artificial potential function method [11]–[13], finite-time control approach [14], etc.

Although most of the existing formation control algorithms of UAVs are elegant and intuitively appealing, they need an implicit assumption that the actuators are able to afford any requested control force. However, available force amplitude is limited owing to the physics characteristic of the actual UAVs. As a result, the assumption may lead to serious discrepancies between commanded input and actual control force, and the control system does not work anymore [15]. Consequently, it is essential to design the formation control algorithms subject to input saturation constraint in this sense. Backstepping control design methodology associated with command filter is an effective tool to overcome the input saturation problem [16]. The designed filter struc-

The associate editor coordinating the review of this manuscript and approving it for publication was Chuxiong Hu.

ture can produce bounded output signals, which guarantees that the actual control input is bounded within the required values to solve the input saturation problem. By incorporating the command filter and adaptive control technique, Farrel *et al.* [17] and Sonneveldt *et al.* [18] solve the input saturation problem in aircraft adaptive flight control design. In [19], Li et al. propose an adaptive backstepping control algorithm for optimal descent tracking. Recently, Zheng et al. present the robust adaptive backstepping control schemes for autonomous attitude cooperative control to overcome the input constraint, model uncertainties, and external disturbances in [20]. In [21], Cui et al. study the distributed consensus control problem by incorporating the command filtered technique into the backstepping design to compensate the effect of input saturation. Yu et al. use the backstepping and the disturbance observer to solve the problems of actuator faults and input saturation in [5]. Zhang et al. address the nonlinear robust close formation control algorithm via the command filtered backstepping technique in [22]. However, it should be noted that, the coordinated control of multiple UAVs formation in the presence of input constraint and model uncertainty is seldom considered yet.

The fault-tolerant capacity of the control algorithms is another fundamental issue in the formation. As a matter of fact, some faults (e.g., a loss of effectiveness or lock-in-place) may occur owing to the malfunction of actuators, which do not only have an adverse impact on control performance but also influent flight safety. To this end, capability of maintaining formation flying in presence of faults is one of the most important issues that need to be addressed, and hence many fault tolerant control approached have been addressed in the past decades. In [23], [24], adaptive sliding mode control strategies are proposed to counteract actuator faults. Liu *et al.* [25] present leader-follower adaptive fault-tolerant control structure along with a collision avoidance strategy. Yu *et al.* [26] address an adaptive fault-tolerant formation control approach and the exponential stability is obtained. In [27], a fault-tolerant control strategy with application to formation flight of multiple UAVs is presented to achieve the finite-time stability. However, the fault tolerant control problem with parameter uncertainty for UAV formation using backstepping method is seldom settled to the best knowledge of the authors. Besides, the external disturbances are not considered in most of the literature.

In this study, the adaptive backstepping formation control schemes are adopted to deal with the input saturation, actuator fault and external disturbance problems during the maneuver. The main contributions of this paper, relative to other works, are summarized as follows:

(1) In the research of input saturation problem, backstepping control combined with command filter is a common approach due to the advantages of simple and reliable characteristic in application. Therefore this method is employed to design formation control algorithms in some literature such as [19], [20]. However, the assumption that no input saturation occurs after finite time is needed to assure the stability in [19], [20]. In this paper, this assumption is removed in the developed adaptive backstepping control algorithm. In addition, the relative position error between the UAV and its neighbors is used to design the virtual velocity error variable, so the information exchanges are utilized in the distributed control strategy. Meanwhile, the adaptive law is designed to estimate the mass of the UAV, and the command filter is developed to counteract the input saturation constraints for implementation.

(2) In this paper, multiple actuator constraints such as input saturation and actuator fault are considered simultaneously. The fault-tolerant term is introduced to eliminate the faults of the actuators, and the distributed fault tolerant backstepping control method is designed. The tracking errors are enforced to the origin, despite of the actuator constraints in the multi-UAV formation system. With the aid of the introduced fault-tolerant term, the corrective control command is executed and the specified formation configuration can be maintained. Different from the existing work of active fault-tolerant control in [5], [23], this paper studies the passive fault-tolerant control for multiple UAVs considering parameter uncertainty and disturbance simultaneously, and the complex fault detection and diagnosis schemes are not required.

(3) The stability of closed-loop control system with the designed controllers is analyzed strictly using Lyapunov method and moreover the asymptotic stability of the closed-loop system is achieved instead of uniform ultimate bounded stability. Meanwhile, in numerical simulation, the position and velocity of the UAVs are perturbed by the zero-mean Gauss white noise to verify the robustness of the presented control approach. The simulation results indicate the favorable performance in presence of the noise.

The rest of the paper is organized as follows. After providing the UAV formation model and basic graph theory in Section II, a distributed adaptive backstepping control law with input saturation constraints for UAV formation is proposed in Section III. After that, a distributed robust fault tolerant formation control law is introduced to deal with external disturbances and actuator fault. Corresponding stability analysis is also provided strictly. Numerical simulation results and conclusions are presented in Section IV and Section V respectively.

II. RELATED FUNDAMENTAL THEORY

A. MATHEMATICAL MODEL OF UAV FORMATION

In this section, the UAV kinematic and dynamic equations are given by the point mass model. For the formation system composed of n UAVs in 3-dimensional space, the kinematics of the ith UAV can be described as the follows [1]

$$\begin{aligned} \dot{x}_i &= V_i \cos\chi_i \cos\gamma_i \\ \dot{y}_i &= V_i \sin\chi_i \cos\gamma_i \\ \dot{z}_i &= V_i \sin\gamma_i \end{aligned} \tag{1}$$

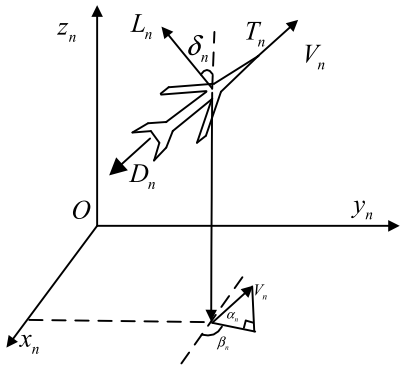

FIGURE 1. The UAV model diagram.

where $i = 1, \cdots, n$ is the index of multiple UAVs. For the i th UAV, (x_i, y_i, z_i) is the position in the inertia frame, V_i is the speed, χ_i is the heading angle, γ_i is the flight path angle. The dynamics of the ith UAV can be described as [1]

$$\begin{aligned}\dot{V}_i &= (T_i - D_i)/m_i - g\sin\gamma_i \\ \dot{\chi}_i &= L_i \sin\phi_i/(m_i V_i \cos\gamma_i) \\ \dot{\gamma}_i &= (L_i\cos\phi_i - m_i g\cos\gamma_i)/(m_i V_i)\end{aligned} \tag{2}$$

where T_i is the engine thrust, L_i and D_i are the vehicle lift and the drag, respectively. m_i, g and ϕ_i are the mass the gravitational constant and the banking angle, respectively. The dynamic model diagram of the UAV is shown in Fig. 1.

Define the control input $\boldsymbol{F}_i = \left[T_i\ L_i\sin\phi_i\ L_i\cos\phi_i\right]^{\mathrm{T}}$, the position $\boldsymbol{p}_i = \left[x_i\ y_i\ z_i\right]^{\mathrm{T}}$, and the velocity $\boldsymbol{v}_i = \left[\dot{x}_i\ \dot{y}_i\ \dot{z}_i\right]^{\mathrm{T}}$. Then from Eq. (1) and (2), it can be obtained that

$$\begin{aligned}\dot{\boldsymbol{p}}_i &= \boldsymbol{v}_i \\ m_i\dot{\boldsymbol{v}}_i &= \boldsymbol{\alpha}_i + m_i\boldsymbol{\varepsilon}_i + \boldsymbol{\beta}_i\boldsymbol{F}_i\end{aligned} \tag{3}$$

where,

$$\boldsymbol{\alpha}_i = \begin{bmatrix} -D_i\cos\chi_i\cos\gamma_i \\ -D_i\sin\chi_i\cos\gamma_i \\ -D_i\sin\gamma_i \end{bmatrix} \tag{4}$$

$$\boldsymbol{\varepsilon}_i = \begin{bmatrix} 0 & 0 & g \end{bmatrix}^{\mathrm{T}} \tag{5}$$

$$\boldsymbol{\beta}_i = \begin{bmatrix} \cos\chi_i\cos\gamma_i & -\sin\chi_i & -\sin\gamma_i\cos\chi_i \\ \sin\chi_i\cos\gamma_i & \cos\chi_i & -\sin\chi_i\sin\gamma_i \\ \sin\gamma_i & 0 & \cos\gamma_i \end{bmatrix} \tag{6}$$

It is easy to obtain that the matrix $\boldsymbol{\beta}_i$ is invertible, and its inverse matrix is

$$\boldsymbol{\beta}_i^{-1} = \begin{bmatrix} \cos\chi_i\cos\gamma_i & \sin\chi_i\cos\gamma_i & \sin\gamma_i \\ -\sin\chi_i & \cos\chi_i & 0 \\ -\sin\gamma_i\cos\chi_i & -\sin\chi_i\sin\gamma_i & \cos\gamma_i \end{bmatrix} \tag{7}$$

B. CONTROL OBJECTIVE

The objective of the paper is then to design the distributed formation controller $\boldsymbol{F}_i$ such that all the UAVs can achieve the designed formation configuration with fault-tolerant ability and input saturation constraint, and the formation system follows a prescribed reference trajectory.

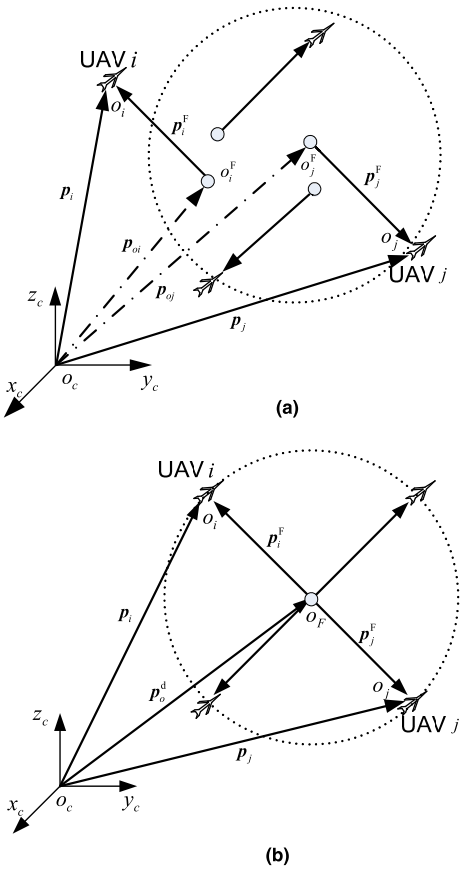

FIGURE 2. Schematic representation of formation keeping. (a) Initial positions without formation. (b) Final positions within formation.

Formation coordination requires that UAVs should maintain their geometric configuration during formation maneuvers. In this study, the desired position of the ith UAV is denoted as $\boldsymbol{p}_i^{\mathrm{d}} = \boldsymbol{p}_o^{\mathrm{d}} + \boldsymbol{p}_i^{\mathrm{F}}$, where $\boldsymbol{p}_o^{\mathrm{d}}$ is the desired position of the formation center, $\boldsymbol{p}_i^{\mathrm{F}}$ is the desired position of the UAV relative to the formation center. So we need to design the controllers $\boldsymbol{F}_i$ to track the desired trajectory such that $\boldsymbol{p}_i \to \boldsymbol{p}_i^{\mathrm{d}}$ and $\dot{\boldsymbol{p}}_i \to \dot{\boldsymbol{p}}_i^{\mathrm{d}}$ as $t \to \infty$. Also note that $\boldsymbol{p}_i \to \boldsymbol{p}_i^{\mathrm{d}}$ and $\boldsymbol{v}_i \to \dot{\boldsymbol{p}}_i^{\mathrm{d}} = \boldsymbol{v}_i^{\mathrm{d}}$ indicate the realization of formation tracking, and $\boldsymbol{p}_i - \boldsymbol{p}_i^{\mathrm{F}} \to \boldsymbol{p}_j - \boldsymbol{p}_j^{\mathrm{F}}$ indicates that the formation keeping is realized during transition, as shown in Fig. 2.

C. BASIC GRAPH THEORY

In this paper, we employ weighted undirected graphs to describe local information exchanges between UAVs in a formation [28]. A weighted undirected graph $\mathrm{G} = (\nu, \varsigma, \boldsymbol{C})$ consists of a node set $\nu = \{1, 2\ldots, n\}$, an edge set $\varsigma \subseteq \nu \times \nu$, and a weighted adjacency matrix $\boldsymbol{C}$. If there exists information transmission from the jth node to the ith node, then there exists an edge from the jth node to the ith node, denoted as $(i, j) \in \varsigma$. In an undirected graph, if $(i, j) \in \varsigma$, then $(j, i) \in \varsigma$. The element of the adjacency matrix $\boldsymbol{C}$ is defined as $c_{ij} = c_{ji} > 0$ if $(i, j) \in \varsigma$ and $i \neq j$, otherwise $c_{ij} = 0$.

III. MAIN RESULTS

A. BACKSTEPPING CONTROL DESIGN

In this part, it is assumed that the actuators of the UAVs can only afford limited control force. In addition, the mass of the UAV are unavailable due to fuel consumption or measure uncertainty. To overcome these problems, a unified adaptive backstepping control algorithm associated with command filter, which is a recursive nonlinear control design approach to use part of system states as virtual control to guarantee the stability of each recursive step, is proposed to achieve the trajectory tracking. Meanwhile, an antiwindup saturation compensator is associated with the controller under input saturation.

Due to the input saturation constraints, the controller can be expressed as

$$\boldsymbol{F}_i = \mathrm{sat}(\boldsymbol{f}_i) \tag{8}$$

where $\mathrm{sat}(\cdot)$ denotes the nonlinear saturation function, which is defined as $\mathrm{sat}(\boldsymbol{y}) = [\,\mathrm{sat}(y_1)\ \mathrm{sat}(y_2)\ \mathrm{sat}(y_3)\,]^{\mathrm{T}}$ and

$$\mathrm{sat}(y_i) = \mathrm{sgn}(y_i)\min\{y_0, |y_i|\} \tag{9}$$

for the vector $\boldsymbol{y} = [\,y_1\ y_2\ y_3\,]^{\mathrm{T}}$, $i = 1, 2, 3$, $\mathrm{sgn}(\cdot)$ is the sign function, $y_0 > 0$ is the bound parameter of the saturation function.

The position and velocity tracking error are defined as $\boldsymbol{e}_{i1} = \boldsymbol{p}_i - \boldsymbol{p}_i^{\mathrm{d}}$ and $\boldsymbol{e}_{i2} = \boldsymbol{v}_i - \boldsymbol{v}_i^{\mathrm{d}}$, respectively. From Eq. (3), the error dynamics equations can be derived as

$$\dot{\boldsymbol{e}}_{i1} = \boldsymbol{e}_{i2} \tag{10}$$

$$m_i\dot{\boldsymbol{e}}_{i2} = \boldsymbol{\alpha}_i + m_i\boldsymbol{\varepsilon}_i + \boldsymbol{\beta}_i\boldsymbol{F}_i - m_i\ddot{\boldsymbol{p}}_i^{\mathrm{d}} \tag{11}$$

Then the adaptive backstepping control algorithms with input saturation can be designed in the following.

Firstly, the backstepping variables are defined

$$\boldsymbol{z}_{i1} = \boldsymbol{\gamma}_i - \boldsymbol{\xi}_i \tag{12}$$

$$\boldsymbol{z}_{i2} = \boldsymbol{e}_{i2} - \boldsymbol{\gamma}_i \tag{13}$$

where $\boldsymbol{\gamma}_i$ is the virtual control to be designed later, $\boldsymbol{\xi}_i$ is the output of a command filter to be defined later. The virtual velocity error $\boldsymbol{\gamma}_i$ is defined as

$$\boldsymbol{\gamma}_i = -k_1\boldsymbol{e}_{i1} - \boldsymbol{r}_i \tag{14}$$

where $k_1 > 0$ is a constant, $\boldsymbol{r}_i = \sum_{j=1}^{n} c_{ij}(\boldsymbol{e}_{i1} - \boldsymbol{e}_{j1})$ represents the information exchanges between the ith UAV and its neighbors, c_{ij} is the ith row and jth column element of the adjacency matrix $\boldsymbol{C}$ with the weighted undirected graph. Then Eq. (10) can be written as

$$\dot{\boldsymbol{e}}_{i1} = \boldsymbol{z}_{i2} - k_1\boldsymbol{e}_{i1} - \boldsymbol{r}_i \tag{15}$$

Let a candidate Lyapunov function be

$$V_1 = \frac{1}{2}\sum_{i=1}^{n}\boldsymbol{e}_{i1}^{\mathrm{T}}\boldsymbol{e}_{i1} + \frac{1}{4}\sum_{i=1}^{n}\sum_{j=1}^{n}c_{ij}(\boldsymbol{e}_{i1} - \boldsymbol{e}_{j1})^{\mathrm{T}}(\boldsymbol{e}_{i1} - \boldsymbol{e}_{j1}) \tag{16}$$

From Eqs. (10)-(15) and $c_{ij} = c_{ji}$, the derivative of V_1 is computed as

$$\begin{aligned}
\dot{V}_1 &= \sum_{i=1}^{n}\dot{\boldsymbol{e}}_{i1}^{\mathrm{T}}\boldsymbol{e}_{i1} + \frac{1}{2}\sum_{i=1}^{n}\sum_{j=1}^{n}c_{ij}(\boldsymbol{e}_{i1} - \boldsymbol{e}_{j1})^{\mathrm{T}}(\dot{\boldsymbol{e}}_{i1} - \dot{\boldsymbol{e}}_{j1}) \\
&= \sum_{i=1}^{n}\boldsymbol{z}_{i2}^{\mathrm{T}}\boldsymbol{e}_{i1} - \sum_{i=1}^{n}k_1\boldsymbol{e}_{i1}^{\mathrm{T}}\boldsymbol{e}_{i1} - \sum_{i=1}^{n}\boldsymbol{e}_{i1}^{\mathrm{T}}\boldsymbol{r}_i + \frac{1}{2}\sum_{i=1}^{n}\sum_{j=1}^{n}c_{ij}\boldsymbol{e}_{i1}^{\mathrm{T}}\dot{\boldsymbol{e}}_{i1} \\
&\quad - \frac{1}{2}\sum_{i=1}^{n}\sum_{j=1}^{n}c_{ij}\boldsymbol{e}_{i1}^{\mathrm{T}}\dot{\boldsymbol{e}}_{j1} - \frac{1}{2}\sum_{i=1}^{n}\sum_{j=1}^{n}c_{ij}\boldsymbol{e}_{j1}^{\mathrm{T}}\dot{\boldsymbol{e}}_{i1} \\
&\quad + \frac{1}{2}\sum_{i=1}^{n}\sum_{j=1}^{n}c_{ij}\boldsymbol{e}_{j1}^{\mathrm{T}}\dot{\boldsymbol{e}}_{j1} \\
&= \sum_{i=1}^{n}\boldsymbol{z}_{i2}^{\mathrm{T}}\boldsymbol{e}_{i1} - \sum_{i=1}^{n}k_1\boldsymbol{e}_{i1}^{\mathrm{T}}\boldsymbol{e}_{i1} - \sum_{i=1}^{n}\boldsymbol{e}_{i1}^{\mathrm{T}}\boldsymbol{r}_i + \frac{1}{2}\sum_{i=1}^{n}\sum_{j=1}^{n}c_{ij}\boldsymbol{e}_{i1}^{\mathrm{T}}\dot{\boldsymbol{e}}_{i1} \\
&\quad - \frac{1}{2}\sum_{j=1}^{n}\sum_{i=1}^{n}c_{ji}\boldsymbol{e}_{i1}^{\mathrm{T}}\dot{\boldsymbol{e}}_{j1} - \frac{1}{2}\sum_{i=1}^{n}\sum_{j=1}^{n}c_{ij}\boldsymbol{e}_{j1}^{\mathrm{T}}\dot{\boldsymbol{e}}_{i1} \\
&\quad + \frac{1}{2}\sum_{j=1}^{n}\sum_{i=1}^{n}c_{ji}\boldsymbol{e}_{j1}^{\mathrm{T}}\dot{\boldsymbol{e}}_{j1} \\
&= \sum_{i=1}^{n}\boldsymbol{z}_{i2}^{\mathrm{T}}\boldsymbol{e}_{i1} - \sum_{i=1}^{n}k_1\boldsymbol{e}_{i1}^{\mathrm{T}}\boldsymbol{e}_{i1} - \sum_{i=1}^{n}\boldsymbol{e}_{i1}^{\mathrm{T}}\boldsymbol{r}_i + \sum_{i=1}^{n}\sum_{j=1}^{n}c_{ij}\boldsymbol{e}_{i1}^{\mathrm{T}}\dot{\boldsymbol{e}}_{i1} \\
&\quad - \sum_{i=1}^{n}\sum_{j=1}^{n}c_{ij}\boldsymbol{e}_{j1}^{\mathrm{T}}\dot{\boldsymbol{e}}_{i1} \\
&= \sum_{i=1}^{n}\boldsymbol{z}_{i2}^{\mathrm{T}}\boldsymbol{e}_{i1} - \sum_{i=1}^{n}k_1\boldsymbol{e}_{i1}^{\mathrm{T}}\boldsymbol{e}_{i1} - \sum_{i=1}^{n}\boldsymbol{e}_{i1}^{\mathrm{T}}\boldsymbol{r}_i + \sum_{i=1}^{n}\boldsymbol{e}_{i2}^{\mathrm{T}}\boldsymbol{r}_i
\end{aligned} \tag{17}$$

Secondly, the estimation of the UAV mass m_i is denoted by $\hat{m}_i$, and the estimation error $\tilde{m}_i = m_i - \hat{m}_i$. The command filter $\boldsymbol{\xi}_i$ is designed as

$$\hat{m}_i\dot{\boldsymbol{\xi}}_i = -k_2\boldsymbol{\xi}_i - \boldsymbol{\beta}_i\Delta\boldsymbol{F}_i \tag{18}$$

where the constant $k_2 > 0$, $\Delta\boldsymbol{F}_i = \boldsymbol{f}_i - \boldsymbol{F}_i$ is the discrepancy between the designed control $\boldsymbol{f}_i$ and the actual control $\boldsymbol{F}_i$. The action of the command filter is to compensate the saturation effect of Eq. (8).

From the definition of $\boldsymbol{z}_{i2}$ and virtual control input Eq. (14), we obtain the dynamics of $\boldsymbol{z}_{i2}$

$$\begin{aligned}
m_i\dot{\boldsymbol{z}}_{i2} &= m_i(\dot{\boldsymbol{e}}_{i2} - \dot{\boldsymbol{z}}_{i1} - \dot{\boldsymbol{\xi}}_i) \\
&= \boldsymbol{\alpha}_i + m_i\boldsymbol{\varepsilon}_i + \boldsymbol{\beta}_i\boldsymbol{F}_i - m_i\ddot{\boldsymbol{p}}_i^{d} - m_i\dot{\boldsymbol{z}}_{i1} - m_i\dot{\boldsymbol{\xi}}_i \\
&= \boldsymbol{\alpha}_i + m_i\boldsymbol{H}_i + \boldsymbol{\beta}_i\boldsymbol{F}_i - \hat{m}_i\dot{\boldsymbol{\xi}}_i - \tilde{m}_i\dot{\boldsymbol{\xi}}_i \\
&= \boldsymbol{\alpha}_i + m_i\boldsymbol{H}_i + \boldsymbol{\beta}_i\boldsymbol{f}_i - \boldsymbol{\beta}_i\Delta\boldsymbol{F}_i - \hat{m}_i\dot{\boldsymbol{\xi}}_i - \tilde{m}_i\dot{\boldsymbol{\xi}}_i \\
&= \boldsymbol{\alpha}_i + m_i\boldsymbol{H}_i + \boldsymbol{\beta}_i\boldsymbol{f}_i + k_2\boldsymbol{\xi}_i - \tilde{m}_i\dot{\boldsymbol{\xi}}_i
\end{aligned} \tag{19}$$

where $\boldsymbol{H}_i = \boldsymbol{\varepsilon}_i - \ddot{\boldsymbol{p}}_i^d - \dot{\boldsymbol{z}}_{i1}$. The control input and adaptive law are proposed as

$$\boldsymbol{f}_i = \boldsymbol{\beta}_i^{-1}(-\boldsymbol{\alpha}_i - \hat{m}_i\boldsymbol{H}_i - k_2\boldsymbol{\xi}_i - k_3\boldsymbol{z}_{i2} - \boldsymbol{e}_{i1} - \sum_{j=1}^{n} c_{ij}(\boldsymbol{e}_{i1} - \boldsymbol{e}_{j1})) \tag{20}$$

$$\dot{\hat{m}} = \lambda_i \boldsymbol{z}_{i2}^{\mathrm{T}}(\boldsymbol{H}_i - \dot{\boldsymbol{\xi}}_i) = \lambda_i \boldsymbol{z}_{i2}^{\mathrm{T}}(\boldsymbol{\varepsilon}_i - \ddot{\boldsymbol{p}}_i^d - \dot{\boldsymbol{\gamma}}_i) \tag{21}$$

where the constant $k_3 > 0$, $\lambda_i > 0$.

Theorem 1: For the UAV formation control system (10)-(11), if the controller is designed as Eqs. (8) and (20), the adaptive law is designed as Eq. (21), the command filter is designed as Eq. (18), and the communication graph is undirected, then the position and velocity tracking error $\boldsymbol{e}_{i1}$ and $\boldsymbol{e}_{i2}$ would converge to zero as the time goes to infinity.

Proof: The Lyapunov function candidate is selected as

$$V_2 = \frac{1}{2}\sum_{i=1}^{n} m_i \boldsymbol{z}_{i2}^{\mathrm{T}}\boldsymbol{z}_{i2} + V_1 + \frac{1}{2\lambda_i}\sum_{i=1}^{n}\tilde{m}_i^2 \tag{22}$$

It is observed that the Lyapunov function $V_2 \geq 0$, and V_2 is a positive-definite function. Differentiating V_2 along the system and using Eqs. (19)-(21) yield that

$$\begin{aligned}
\dot{V}_2 &= \sum_{i=1}^{n} m_i \boldsymbol{z}_{i2}^{\mathrm{T}}\dot{\boldsymbol{z}}_{i2} + \dot{V}_1 + \sum_{i=1}^{n}\frac{1}{\lambda_i}\tilde{m}_i\dot{\tilde{m}}_i \\
&= \sum_{i=1}^{n} \boldsymbol{z}_{i2}^{\mathrm{T}}\left(\boldsymbol{\alpha}_i + m_i\boldsymbol{H}_i + \boldsymbol{\beta}_i\boldsymbol{f}_i - \tilde{m}_i\dot{\xi}_i + k_2\xi_i\right) + \sum_{i=1}^{n}\boldsymbol{z}_{i2}^{\mathrm{T}}\boldsymbol{e}_{i1} \\
&\quad - \sum_{i=1}^{n} k_1\boldsymbol{e}_{i1}^{\mathrm{T}}\boldsymbol{e}_{i1} - \sum_{i=1}^{n}\boldsymbol{e}_{i1}^{\mathrm{T}}\boldsymbol{r}_i + \sum_{i=1}^{n}\boldsymbol{e}_{i2}^{\mathrm{T}}\boldsymbol{r}_i - \sum_{i=1}^{n}\frac{1}{\lambda_i}\tilde{m}_i\dot{\hat{m}}_i \\
&= \sum_{i=1}^{n} \boldsymbol{z}_{i2}^{\mathrm{T}}\left(\tilde{m}_i\boldsymbol{H}_i - \tilde{m}_i\dot{\boldsymbol{\xi}}_i - k_3\boldsymbol{z}_{i2} - \boldsymbol{r}_i\right) - \sum_{i=1}^{n} k_1\boldsymbol{e}_{i1}^{\mathrm{T}}\boldsymbol{e}_{i1} \\
&\quad - \sum_{i=1}^{n}\boldsymbol{e}_{i1}^{\mathrm{T}}\boldsymbol{r}_i + \sum_{i=1}^{n}\boldsymbol{e}_{i2}^{\mathrm{T}}\boldsymbol{r}_i - \sum_{i=1}^{n}\tilde{m}_i\boldsymbol{z}_{i2}^{\mathrm{T}}\left(\boldsymbol{H}_i - \dot{\xi}_i\right) \\
&= -k_3\sum_{i=1}^{n}\boldsymbol{z}_{i2}^{\mathrm{T}}\boldsymbol{z}_{i2} - k_1\sum_{i=1}^{n}\boldsymbol{e}_{i1}^{\mathrm{T}}\boldsymbol{e}_{i1} - \sum_{i=1}^{n}\boldsymbol{e}_{i1}^{\mathrm{T}}\boldsymbol{r}_i \\
&\quad + \sum_{i=1}^{n}\left(-k_1\boldsymbol{e}_{i1} - \boldsymbol{r}_i\right)^{\mathrm{T}}\boldsymbol{r}_i \\
&= -k_3\sum_{i=1}^{n}\boldsymbol{z}_{i2}^{\mathrm{T}}\boldsymbol{z}_{i2} - k_1\sum_{i=1}^{n}\boldsymbol{e}_{i1}^{\mathrm{T}}\boldsymbol{e}_{i1} - \sum_{i=1}^{n}\boldsymbol{r}_i^{\mathrm{T}}\boldsymbol{r}_i \\
&\quad - \frac{k_1+1}{2}\sum_{i=1}^{n}\sum_{j=1}^{n} c_{ij}\left(\boldsymbol{e}_{i1} - \boldsymbol{e}_{j1}\right)^{\mathrm{T}}\left(\boldsymbol{e}_{i1} - \boldsymbol{e}_{j1}\right) \\
&\leq 0
\end{aligned} \tag{23}$$

So $\boldsymbol{z}_{i2}, \tilde{m}_i, \boldsymbol{r}_i$ and $\boldsymbol{e}_{i1}$ are all bounded. From Eqs. (19) and (20), we obtain that

$$m_i\dot{\boldsymbol{z}}_{i2} = \tilde{m}_i\boldsymbol{H}_i - k_3\boldsymbol{z}_{i2} - \boldsymbol{e}_{i1} - \boldsymbol{r}_i - \tilde{m}_i\dot{\boldsymbol{\xi}}_i \tag{24}$$

Thus $\dot{\boldsymbol{z}}_{i2}$ is also bounded. Differentiating Eq. (23), we can obtain that $\ddot{V}_2$ is bounded due to the fact that $\boldsymbol{z}_{i2}, \dot{\boldsymbol{z}}_{i2}, \boldsymbol{e}_{i1}$ and $\dot{\boldsymbol{e}}_{i1}$ are all bounded. Therefore $\dot{V}_2$ is uniformly continuous. From Barbalat's Lemma [29], it concludes that $\dot{V}_2$ converge to zero. Consequently, $\boldsymbol{z}_{i2}, \boldsymbol{r}_i$ and $\boldsymbol{e}_{i1}$ converge to zero as the time goes to infinity. Therefore, $\boldsymbol{e}_{i1} \to 0$ and $\boldsymbol{e}_{i2} = \boldsymbol{z}_{i2} - k_1\boldsymbol{e}_{i1} - \boldsymbol{r}_i \to 0$ as $t \to \infty$.

Remark 1: Compared with the results in [19], [20], our results do not need the assumption that no input saturation occur after finite time. Moreover the asymptotic stability is achieved under the proposed controllers instead of uniform ultimate bounded stability. This is the main merit and innovation of the presented control approach.

Remark 2: Note that $\boldsymbol{e}_{i1} - \boldsymbol{e}_{j1} = \boldsymbol{p}_i - \boldsymbol{p}_j - (\boldsymbol{p}_i^{\mathrm{d}} - \boldsymbol{p}_j^{\mathrm{d}})$ and $\boldsymbol{p}_i^{\mathrm{d}} - \boldsymbol{p}_j^{\mathrm{d}}$ is related to the formation shape, thus the positions of the UAV's neighbors should be utilized. From this point of view, the controller (20) is distributed. According to the preceding analysis, the controller (20) can be viewed as the sum of station-keeping and formation-keeping behaviors. Specifically, the first five items of controller (20) are station keeping terms and are intended to drive the UAV to its final position. The last one item, generated by consensus algorithms similar to those of [28], is formation-keeping terms and intends to help the UAVs maintain formation configuration during the maneuver.

Remark 3: In the proof of Theorem 1, it is only assumed that the interaction graph is undirected and the connectedness of the graph is not needed. Even when there is no information transmission, the conclusion is also valid. In such a case, the controller (20) becomes centralized trajectory tracking controller without any information interactions.

B. ADAPTIVE CONTROLLER WITH ACTUATOR FAULTS AND DISTURBANCES

Note that we do not consider the external disturbances and actuator faults currently. However, the UAV would inevitably suffer unknown bounded external disturbances owing to uncertain outdoor flying environment, such as wind gust, the payload mass variation, nonlinear aerodynamic friction, and so on. Moreover, the tremendous and complicated formation system may emerge various faults easily, and the impact of the faults may lead to the failure of overall formation system, even when the impact of faults could be a slight reduction in efficiency. In this case, we assume that the actuators of the UAV may lose its effectiveness partially and the external disturbances are also considered.

Without going into the details of the possible nature of actuator faults, the UAV error dynamics model (11) with actuator faults and disturbances is given by

$$m_i\dot{\boldsymbol{e}}_{i2} = \boldsymbol{\alpha}_i + m_i\boldsymbol{\varepsilon}_i + \boldsymbol{d}_i + \boldsymbol{\Gamma}_i\boldsymbol{\beta}_i\boldsymbol{F}_i - m_i\ddot{\boldsymbol{p}}_i^d \tag{25}$$

where $\boldsymbol{d}_i = [d_i^{(1)}\ d_i^{(2)}\ d_i^{(3)}]$ is the unknown external disturbances bounded with $\|\boldsymbol{d}_i\|_\infty \leq D_i$, and $D_i > 0$ is an unknown constant. The actuator effectiveness $\boldsymbol{\Gamma}_i = \mathrm{diag}\{\delta_i^{(1)}, \delta_i^{(2)}, \delta_i^{(3)}\}$ is a diagonal time-varying matrix, which satisfies $0 < \tau_i \leq \min\{\delta_i^{(1)}(t), \delta_i^{(2)}(t), \delta_i^{(3)}(t)\} \leq 1$. Note that the case $\delta_i^{(j)} = 1 (1 \leq j \leq 3)$ means that the jth actuator of the ith UAV

works normally, and $0 < \tau_i \leq \delta_i^{(j)} < 1$ represents that the ith actuator has partially lost its effectiveness, but it still works all the time.

The robust fault-tolerant adaptive controllers are proposed as

$$\boldsymbol{F}_i = \boldsymbol{F}_i^{(1)} + \boldsymbol{F}_i^{(2)} + \boldsymbol{F}_i^{(3)} \tag{26}$$

$$\boldsymbol{F}_i^{(1)} = \boldsymbol{\beta}_i^{-1}(-\boldsymbol{\alpha}_i - \hat{m}_i \boldsymbol{Y}_i - k_3 \boldsymbol{z}_{i2} - \boldsymbol{e}_{i1} - \sum_{j=1}^{n} c_{ij}(\boldsymbol{e}_{i1} - \boldsymbol{e}_{j1})) \tag{27}$$

$$\boldsymbol{F}_i^{(2)} = -\boldsymbol{\beta}_i^{-1} \mathrm{diag}\{\hat{\theta}_i^{(1)}, \hat{\theta}_i^{(2)}, \hat{\theta}_i^{(3)}\} \mathrm{sgn}(\boldsymbol{z}_{i2}) \tag{28}$$

$$\boldsymbol{F}_i^{(3)} = -\boldsymbol{\beta}_i^{-1} \hat{D}_i \mathrm{sgn}(\boldsymbol{z}_{i2}) \tag{29}$$

$$\dot{\hat{m}} = \lambda_i \boldsymbol{z}_{i2}^{\mathrm{T}} \boldsymbol{Y}_i \tag{30}$$

where $\boldsymbol{Y}_i = \boldsymbol{\varepsilon}_i - \ddot{\boldsymbol{p}}_i^d + k_1 \boldsymbol{e}_{i2}$, $\boldsymbol{F}_i^{(1)}$ is the normal controller, $\boldsymbol{F}_i^{(2)}$ is the adaptive compensation control term that is to countervail the partial failure of actuators, $\hat{\theta}_i^{(j)} (1 \leq j \leq 3)$ is the estimate of $\theta_i^{(j)}$, $\theta_i^{(j)}$ is a constant parameter to be defined. The adaptive update law of $\hat{\theta}_i^{(j)}$ is designed as

$$\dot{\hat{\theta}}_i^{(j)} = \gamma_i^{(j)} \left| z_{i2}^{(j)} \right| \tag{31}$$

where $z_{i2}^{(j)}$ is the j th element of $\boldsymbol{z}_{i2}$, $\gamma_i^{(j)} > 0$ is a gain coefficient. And $\boldsymbol{F}_i^{(3)}$ is the disturbance rejection term to eliminate the external disturbances, where $\hat{D}_i$ is the estimation of D_i. The adaptive update law of $\hat{D}_i$ is designed as

$$\dot{\hat{D}}_i = \delta_i \left\| \boldsymbol{z}_{i2} \right\|_1 \tag{32}$$

where $\delta_i > 0$ is a gain coefficient. From Eqs. (26)-(29), it follows that

$$\begin{aligned} \boldsymbol{\Gamma}_i \boldsymbol{\beta}_i \boldsymbol{F}_i &= \boldsymbol{\Gamma}_i \boldsymbol{\beta}_i \boldsymbol{F}_i \\ &= \boldsymbol{\beta}_i \boldsymbol{F}_i - (\boldsymbol{I}_3 - \boldsymbol{\Gamma}_i) \boldsymbol{\beta}_i \boldsymbol{F}_i \\ &= -\boldsymbol{\alpha}_i - \hat{m}_i \boldsymbol{Y}_i - k_3 \boldsymbol{z}_{i2} - \boldsymbol{e}_{i1} - \boldsymbol{r}_i - \hat{D}_i \, \mathrm{sgn}(\boldsymbol{z}_{i2}) \\ &\quad - \mathrm{diag}\left\{\hat{\theta}_i^{(1)}, \hat{\theta}_i^{(2)}, \hat{\theta}_i^{(3)}\right\} \mathrm{sgn}(\boldsymbol{z}_{i2}) - (\boldsymbol{I}_3 - \boldsymbol{\Gamma}_i) \boldsymbol{\beta}_i \boldsymbol{F}_i \end{aligned} \tag{33}$$

According to Eqs. (25) and (33), it is derived that

$$\begin{aligned} m_i \dot{\boldsymbol{z}}_{i2} &= m_i (\dot{\boldsymbol{e}}_{i2} + k_1 \dot{\boldsymbol{e}}_{i1}) \\ &= \boldsymbol{\alpha}_i + m_i \boldsymbol{e}_i + \boldsymbol{d}_i + \boldsymbol{\Gamma}_i \boldsymbol{\beta}_i \boldsymbol{F}_i - m_i \ddot{\boldsymbol{p}}_i^d + k_1 m_i \boldsymbol{e}_{i2} \\ &= \boldsymbol{\alpha}_i + m_i \boldsymbol{Y}_i + \boldsymbol{d}_i + \boldsymbol{\Gamma}_i \boldsymbol{\beta}_i \boldsymbol{F}_i \\ &= \tilde{m}_i \boldsymbol{Y}_i + \boldsymbol{d}_i - k_3 \boldsymbol{z}_{i2} - \boldsymbol{e}_{i1} - (\boldsymbol{I}_3 - \boldsymbol{\Gamma}_i) \boldsymbol{\beta}_i \boldsymbol{F}_i - \hat{D}_i \, \mathrm{sgn}(\boldsymbol{z}_{i2}) \\ &\quad - \sum_{j=1}^{n} c_{ij} (\boldsymbol{e}_{i1} - \boldsymbol{e}_{j1}) - diag\left\{\hat{\theta}_i^{(1)}, \hat{\theta}_i^{(2)}, \hat{\theta}_i^{(3)}\right\} \mathrm{sgn}(\boldsymbol{z}_{i2}) \end{aligned} \tag{34}$$

It is assumed that the control force is bounded in practice, which is previously assumed to be bounded in [15], [25]–[27], namely $\left\| \boldsymbol{F}_i \right\|_\infty \leq l_f$. Let

$$\boldsymbol{M_i} = [M_i^{(1)} \quad M_i^{(2)} \quad M_i^{(3)}]^{\mathrm{T}} = -(\boldsymbol{I}_3 - \boldsymbol{\Gamma}_i) \boldsymbol{\beta}_i \boldsymbol{F}_i$$

Then $M_i^{(j)}$ $(j = 1, 2, 3)$ is bounded and expressed as

$$\left| M_i^{(j)} \right| \leq 3 l_f \left(1 - \delta_i^{(j)}\right) \leq \theta_i^{(j)} \tag{35}$$

where $\theta_i^{(j)}$ is the unknown constant upper bound of $3 l_f (1 - \delta_i^{(j)})$.

Theorem 2: For the UAV formation control system Eqs. (10) and (25) with actuator faults and external disturbances, the adaptive fault tolerant controller is designed as Eqs. (26)-(29), the adaptive laws are designed as Eqs. (30), (31) and (32). If the communication graph is undirected, the position and velocity tracking error $\boldsymbol{e}_{i1}$ and $\boldsymbol{e}_{i2}$ would converge to zero as the time goes to infinity.

Proof: The Lyapunov function candidate is selected as

$$V_3 = V_2 + \frac{1}{2\delta_i} \sum_{i=1}^{n} \tilde{D}_i^2 + \sum_{i=1}^{n} \sum_{j=1}^{3} \frac{\left(\tilde{\theta}_i^{(j)}\right)^2}{2\gamma_i^{(j)}} \tag{36}$$

where $\tilde{D}_i = D_i - \hat{D}_i$. From Eqs. (30), (34) and (35), we can obtain that

$$\begin{aligned} \dot{V}_2 &= \sum_{i=1}^{n} m_i \boldsymbol{z}_{i2}^{\mathrm{T}} \dot{\boldsymbol{z}}_{i2} + \dot{V}_1 + \frac{1}{\lambda_i} \sum_{i=1}^{n} \tilde{m}_i \dot{\tilde{m}}_i \\ &= -k_3 \sum_{i=1}^{n} \boldsymbol{z}_{i2}^{\mathrm{T}} \boldsymbol{z}_{i2} - k_1 \sum_{i=1}^{n} \boldsymbol{e}_{i1}^{\mathrm{T}} \boldsymbol{e}_{i1} - \sum_{i=1}^{n} \boldsymbol{e}_{i1}^{\mathrm{T}} \boldsymbol{r}_i + \sum_{i=1}^{n} \tilde{m}_i \boldsymbol{z}_{i2}^{\mathrm{T}} \boldsymbol{Y}_i \\ &\quad + \sum_{i=1}^{n} \boldsymbol{z}_{i2}^{\mathrm{T}} \boldsymbol{d}_i + \sum_{i=1}^{n} \boldsymbol{e}_{i2}^{\mathrm{T}} \boldsymbol{r}_i - \sum_{i=1}^{n} \boldsymbol{z}_{i2}^{\mathrm{T}} \boldsymbol{r}_i + \sum_{i=1}^{n} \boldsymbol{z}_{i2}^{\mathrm{T}} (\boldsymbol{I}_3 - \boldsymbol{\Gamma}_i) \boldsymbol{\beta}_i \boldsymbol{F}_i \\ &\quad - \sum_{i=1}^{n} \sum_{j=1}^{3} \hat{\theta}_i^{(j)} \left| z_{i2}^{(j)} \right| - \sum_{i=1}^{n} \hat{D}_i \left\| \boldsymbol{z}_{i2} \right\|_1 - \sum_{i=1}^{n} \tilde{m}_i \boldsymbol{z}_{i2}^{\mathrm{T}} \boldsymbol{Y}_i \\ &\leq -k_3 \sum_{i=1}^{n} \boldsymbol{z}_{i2}^{\mathrm{T}} \boldsymbol{z}_{i2} - k_1 \sum_{i=1}^{n} \boldsymbol{e}_{i1}^{\mathrm{T}} \boldsymbol{e}_{i1} - \sum_{i=1}^{n} \boldsymbol{e}_{i1}^{\mathrm{T}} \boldsymbol{r}_i + \sum_{i=1}^{n} \tilde{D}_i \left\| \boldsymbol{z}_{i2} \right\|_1 \\ &\quad + \sum_{i=1}^{n} \sum_{j=1}^{3} \theta_i^{(j)} \left| z_{i2}^{(j)} \right| - \sum_{i=1}^{n} \sum_{j=1}^{3} \hat{\theta}_i^{(j)} \left| z_{i2}^{(j)} \right| - \sum_{i=1}^{n} (k_1 \boldsymbol{e}_{i1} + \boldsymbol{r}_i)^{\mathrm{T}} \boldsymbol{r}_i \\ &= -k_3 \sum_{i=1}^{n} \boldsymbol{z}_{i2}^{\mathrm{T}} \boldsymbol{z}_{i2} - k_1 \sum_{i=1}^{n} \boldsymbol{e}_{i1}^{\mathrm{T}} \boldsymbol{e}_{i1} + \sum_{i=1}^{n} \tilde{D}_i \| \boldsymbol{z}_{i2\|_1} - \sum_{i=1}^{n} \boldsymbol{r}_i^{\mathrm{T}} \boldsymbol{r}_i \\ &\quad + \sum_{i=1}^{n} \sum_{j=1}^{3} \tilde{\theta}_i^{(j)} \left| z_{i2}^{(j)} \right| - \frac{k_1 + 1}{2} \sum_{i=1}^{n} \sum_{j=1}^{n} \\ &\quad \times c_{ij} \left(\boldsymbol{e}_{i1} - \boldsymbol{e}_{j1}\right)^{\mathrm{T}} \left(\boldsymbol{e}_{i1} - \boldsymbol{e}_{j1}\right) \end{aligned} \tag{37}$$

Differentiating V_3 and using Eqs. (31), (32) and (37) yield that

$$\begin{aligned} \dot{V}_3 &= \dot{V}_2 - \frac{1}{\delta_i} \sum_{i=1}^{n} \tilde{D}_i \dot{D}_i - \sum_{i=1}^{n} \sum_{j=1}^{3} \frac{\tilde{\theta}_i^{(j)}}{\gamma_i^{(j)}} \dot{\hat{\theta}}_i^{(j)} \\ &\leq -k_3 \sum_{i=1}^{n} \boldsymbol{z}_{i2}^{\mathrm{T}} \boldsymbol{z}_{i2} - k_1 \sum_{i=1}^{n} \boldsymbol{e}_{i1}^{\mathrm{T}} \boldsymbol{e}_{i1} + \sum_{i=1}^{n} \tilde{D}_i \left\| \boldsymbol{z}_{i2} \right\|_1 - \sum_{i=1}^{n} \boldsymbol{r}_i^{\mathrm{T}} \boldsymbol{r}_i \end{aligned}$$

$$
\begin{aligned}
&+\sum_{i=1}^{n}\sum_{j=1}^{3}\tilde{\theta}_i^{(j)}\left|z_{i2}^{(j)}\right|-\frac{k_1+1}{2}\sum_{i=1}^{n}\sum_{j=1}^{n}\\
&\times c_{ij}\left(\boldsymbol{e}_{i1}-\boldsymbol{e}_{j1}\right)^{\mathrm{T}}\left(\boldsymbol{e}_{i1}-\boldsymbol{e}_{j1}\right)\\
&-\sum_{i=1}^{n}\tilde{D}_i\left\|z_{i2}\right\|_1-\sum_{i=1}^{n}\sum_{j=1}^{3}\tilde{\theta}_i^{(j)}\left|z_{i2}^{(j)}\right|\\
=&-k_3\sum_{i=1}^{n}z_{i2}^{\mathrm{T}}z_{i2}-k_1\sum_{i=1}^{n}\boldsymbol{e}_{i1}^{\mathrm{T}}\boldsymbol{e}_{i1}-\sum_{i=1}^{n}v_i^{\mathrm{T}}v_i\\
&-\frac{k_1+1}{2}\sum_{i=1}^{n}\sum_{j=1}^{n}c_{ij}\left(\boldsymbol{e}_{i1}-\boldsymbol{e}_{j1}\right)^{\mathrm{T}}\left(\boldsymbol{e}_{i1}-\boldsymbol{e}_{j1}\right)\\
\le&\ 0
\end{aligned}
\tag{38}
$$

It follows that V_3 is bounded, and $z_{i2}, \tilde{m}_i, \boldsymbol{v}_i, \tilde{\theta}_i^{(j)}, \tilde{D}_i, \boldsymbol{e}_{i1} \in L_\infty$ are all bounded. From Eq. (34), we can obtain that $\dot{z}_{i2} \in L_\infty$, $\dot{\boldsymbol{e}}_{i1} = z_{i2} - k_1\boldsymbol{e}_{i1} - \boldsymbol{v}_i \in L_\infty$. Meanwhile, the fact that V_3 is bounded and $\dot{V}_3 \le 0$ implies $\lim_{t\to\infty}\int_0^t \dot{V}_3(\tau)\mathrm{d}\tau < \infty$, thus

$$
k_3\sum_{i=1}^{n}\int_0^{\infty}z_{i2}^{\mathrm{T}}z_{i2}\mathrm{d}\tau+k_1\sum_{i=1}^{n}\int_0^{\infty}\boldsymbol{e}_{i1}^{\mathrm{T}}\boldsymbol{e}_{i1}\mathrm{d}\tau\le\lim_{t\to\infty}\int_0^t\dot{V}_3(\tau)\mathrm{d}\tau<\infty
\tag{39}
$$

In other words, $z_{i2}, \quad \boldsymbol{e}_{i1} \in L_2$. From Barbalat's Lemma [29], it concludes that z_{i2} and $\boldsymbol{e}_{i1}$ converge to zero as the time goes to infinity.

Remark 4: The proposed controllers (26)-(29) are discontinuous because of the term sgn(z_{i2}), which may bring about undesirable chattering in the vicinity of switching. This problem can be alleviated by replacing the discontinuous function sgn(z_{i2}) by a continuous function tanh(z_{i2}) or sat(z_{i2}).

IV. SIMULATION RESULTS

A. BASIC PARAMETER SETTINGS

Simulation results are presented in this section to support the proposed methods. A scenario with four UAVs in the formation is considered. The gravity constant is $g = 9.81$ kg/m^2. The drag in the UAV model Eq. (2) is calculated by [3]

$$
D_i=\frac{0.5\rho(V_i-V_{wi})^2SC_{D0}+2k_dk_n^2L^2/g^2}{\rho(V_i-V_{wi})^2S}
$$

where ρ is the atmospheric density and equal to 1.225 kg/m^3, V_{wi} is the gust, S is the wing area and equal to 1.37 m^2, C_{D0} is the zero-lift drag coefficient and equal to 0.02, k_d is the induced drag coefficient and equal to 0.1, and k_n is the load-factor effectiveness and equal to 1.

The mass of the UAVs are $m_1 = 1.5$ kg, $m_2 = 2$kg, $m_3 = 1.8$kg, $m_4 = 1.6$kg, respectively. The initial values of the position and velocity are given by

$$
\begin{aligned}
\boldsymbol{p}_1(0)&=\begin{bmatrix}-58 & 62 & 584\end{bmatrix}^{\mathrm{T}}\mathrm{m},\\
\boldsymbol{v}_1(0)&=\begin{bmatrix}5 & 5\sqrt{2} & 5\sqrt{2}\end{bmatrix}^{\mathrm{T}}\mathrm{m/s}\\
\boldsymbol{p}_2(0)&=\begin{bmatrix}-62 & 60 & 580\end{bmatrix}^{\mathrm{T}}\mathrm{m},\\
\boldsymbol{v}_2(0)&=\begin{bmatrix}\frac{11}{4} & \frac{11\sqrt{3}}{4} & \frac{11\sqrt{3}}{2}\end{bmatrix}^{\mathrm{T}}\mathrm{m/s}
\end{aligned}
$$

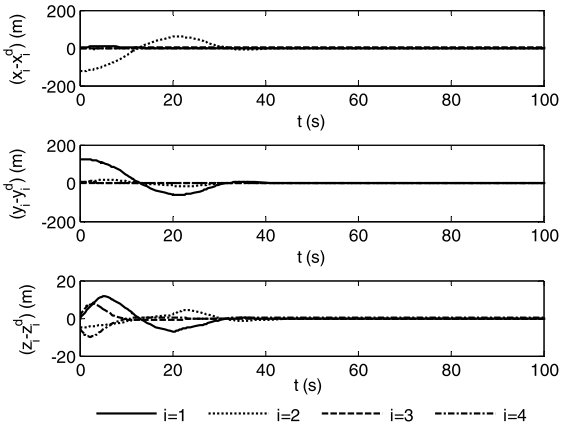

FIGURE 3. Position tracking errors with controller (20).

$$
\begin{aligned}
\boldsymbol{p}_3(0)&=\begin{bmatrix}-60 & -60 & 416\end{bmatrix}^{\mathrm{T}}\mathrm{m},\\
\boldsymbol{v}_3(0)&=\begin{bmatrix}6 & 6 & 6\sqrt{2}\end{bmatrix}^{\mathrm{T}}\mathrm{m/s}\\
\boldsymbol{p}_4(0)&=\begin{bmatrix}55 & 63 & 410\end{bmatrix}^{\mathrm{T}}\mathrm{m},\\
\boldsymbol{v}_4(0)&=\begin{bmatrix}\frac{5\sqrt{3}}{2} & \frac{15}{2} & 5\end{bmatrix}^{\mathrm{T}}\mathrm{m/s}
\end{aligned}
$$

The desired positions of the UAVs relative to the formation center are given by

$$
\begin{aligned}
\boldsymbol{p}_{1\mathrm{F}}(0)&=\begin{bmatrix}-60 & -60 & 60\sqrt{2}\end{bmatrix}^{\mathrm{T}}m,\\
\boldsymbol{p}_{2\mathrm{F}}(0)&=\begin{bmatrix}60 & 60 & 60\sqrt{2}\end{bmatrix}^{\mathrm{T}}m,\\
\boldsymbol{p}_{3\mathrm{F}}(0)&=\begin{bmatrix}-60 & -60 & -60\sqrt{2}\end{bmatrix}^{\mathrm{T}}m,\\
\boldsymbol{p}_{4\mathrm{F}}(0)&=\begin{bmatrix}60 & 60 & -60\sqrt{2}\end{bmatrix}^{\mathrm{T}}m.
\end{aligned}
$$

The desired position and velocity of the formation center are given by

$$
\begin{aligned}
\boldsymbol{p}_o^{\mathrm{d}}&=\begin{bmatrix}0 & 100t & 500\end{bmatrix}^{\mathrm{T}}m,\\
\boldsymbol{v}_o^{\mathrm{d}}&=\dot{\boldsymbol{p}}_o^{\mathrm{d}}.
\end{aligned}
$$

Then the desired position and velocity of each UAV are given by

$$
\begin{aligned}
\boldsymbol{p}_i^{\mathrm{d}}&=\boldsymbol{p}_i^{\mathrm{F}}+\boldsymbol{p}_o^{\mathrm{d}},\\
\boldsymbol{v}_i^{\mathrm{d}}&=\dot{\boldsymbol{p}}_i^{\mathrm{d}},\quad i=1,2,3,4.
\end{aligned}
$$

The sensor noise is considered in the simulations. Assume that the position and velocity of UAVs are perturbed by a zero-mean Gauss white noise. The white noise has a variance of 0.0002. When the proposed controllers are implemented, the weighted adjacency matrix associated with the communication topology is chosen as

$$
C=\left[c_{ij}\right]_{4\times4}=\begin{bmatrix}0 & 1.2 & 0 & 1\\ 1.2 & 0 & 0 & 0\\ 0 & 0 & 0 & 0.8\\ 1 & 0 & 0.8 & 0\end{bmatrix}
$$

The parameters of the controller (20) are chosen as $k_1 = 0.2$, $k_2 = 8$, $k_3 = 150$, $\lambda_i = 0.001$, the initial values

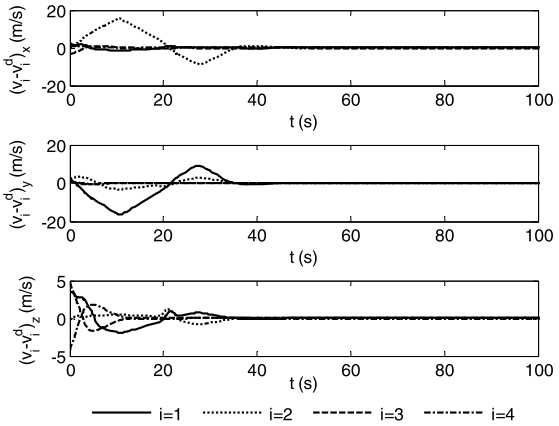

FIGURE 4. Velocity tracking errors with controller (20).

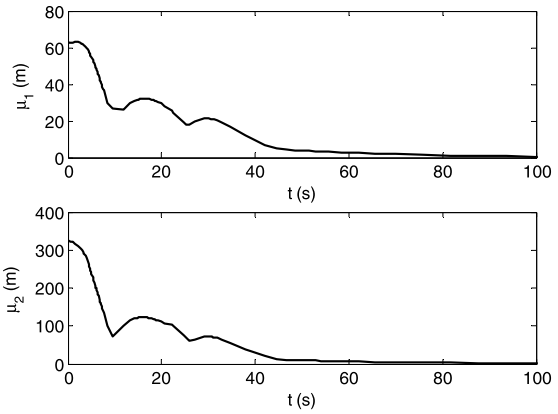

FIGURE 5. Formation tracking and keeping performance with controller (20).

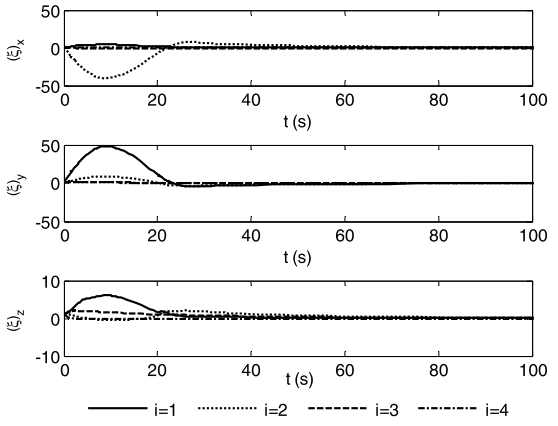

FIGURE 6. Command filter with controller (20).

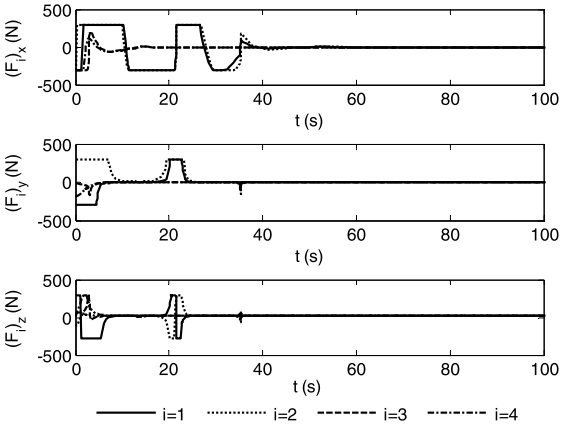

FIGURE 7. Actual control force with controller (20).

of $\hat{m}_i$ in Eq. (21) and $\boldsymbol{\xi}_i$ in Eq. (18) are chosen as $\hat{m}_1(0) = 2$ kg, $\hat{m}_2(0) = 2.1$ kg, $\hat{m}_3(0) = 2.2$ kg, $\hat{m}_4(0) = 1.8$ kg, $\boldsymbol{\xi}_i(0) = [1 \;\; 1 \;\; 1]^{\mathrm{T}}$. The parameter of the saturation function in Eq. (8) is chosen as $y_0 = 300$. The parameters of controller (27) are chosen as $k_1 = 0.2$, $k_2 = 8$, $k_3 = 150$, $\lambda_i = 0.001$, the initial values of $\hat{m}_i$ in Eq. (21), $\hat{D}_i$ in Eq. (32) and $\hat{\theta}_i^{(j)}$ in Eq. (31) are chosen as $\hat{m}_1(0) = 2$ kg, $\hat{m}_2(0) = 2.1$ kg, $\hat{m}_3(0) = 2.2$ kg, $\hat{m}_4(0) = 1.8$ kg, $\hat{D}_1(0) = 2$, $\hat{D}_2(0) = 3$, $\hat{D}_3(0) = 4$, $\hat{D}_4(0) = 5$, $\hat{\theta}_i^{(j)} = 1$. The actuator effectiveness is selected as

$$\delta_i^{(1)}(t) = \begin{cases} 1 & t \le 10 \\ 1 - 0.1(i+1)e^{-(t-10)} & t \ge 10 \end{cases}$$

$$\delta_i^{(2)}(t) = \begin{cases} 1 & t \le 15 \\ 1 - 0.1e^{-0.5i(t-15)} & t \ge 15 \end{cases}$$

$$\delta_i^{(3)}(t) = \begin{cases} 1 & t \le 20 \\ 1 - 0.05(i+2)e^{-0.2(t-10)} & t \ge 20 \end{cases}$$

The external disturbances are chosen as

$$\boldsymbol{d}_i = \begin{bmatrix} (i+1)\cos(0.1t) + 2i\sin(0.2t) \\ 2i\cos(0.2t) + 3i \\ (i-3)\sin(0.1t) - 2i \end{bmatrix}^{\mathrm{T}} \mathrm{N} \quad \text{for } i = 1, 2, 3, 4.$$

To describe the formation tracking and formation keeping performance of the UAVs quantitatively, the formation tracking error μ_1 and formation keeping error μ_2 are defined as

$$\mu_1 = \frac{1}{4}\sum_{i=1}^{4} \|\boldsymbol{e}_i\|_2$$

$$\mu_2 = \left|\left\|\boldsymbol{p}_1 - \boldsymbol{p}_2\right\|_2 - \left\|\boldsymbol{p}_1 - \boldsymbol{p}_3\right\|_2\right| + \left|\left\|\boldsymbol{p}_1 - \boldsymbol{p}_2\right\|_2 - \left\|\boldsymbol{p}_3 - \boldsymbol{p}_4\right\|_2\right| + \left|\left\|\boldsymbol{p}_2 - \boldsymbol{p}_4\right\|_2 - \left\|\boldsymbol{p}_3 - \boldsymbol{p}_4\right\|_2\right|$$

According to the assignment of the desired formation configuration, it is clear that smaller μ_1 and μ_2 during formation maneuver mean the better performance of formation tracking and formation maintenance.

B. THE SIMULATION RESULTS OF CONTROLLER (20)

The simulation results of the backstepping controller (20) are demonstrated in Fig. 3-Fig. 7, respectively. It can be seen from Fig. 3 that the position errors $\boldsymbol{e}_{i1}$ converges to zero eventually, which shows that the control objective is achieved. In addition, the UAVs reach the desired position and follow the desired reference trajectory finally. The responses of the velocity error $\boldsymbol{e}_{i2}$ are shown in Fig. 4. It can be observed that the velocity error decays quickly as well. Fig. 5 illustrates

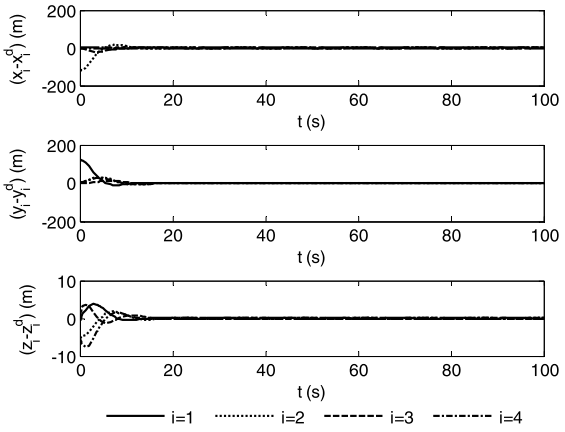

FIGURE 8. Position tracking errors with controller (26).

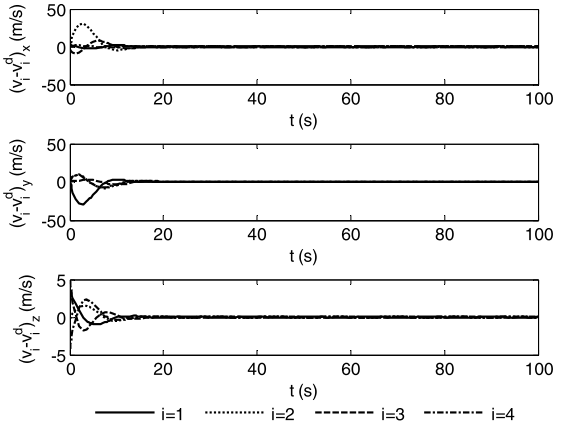

FIGURE 9. Velocity tracking errors with controller (26).

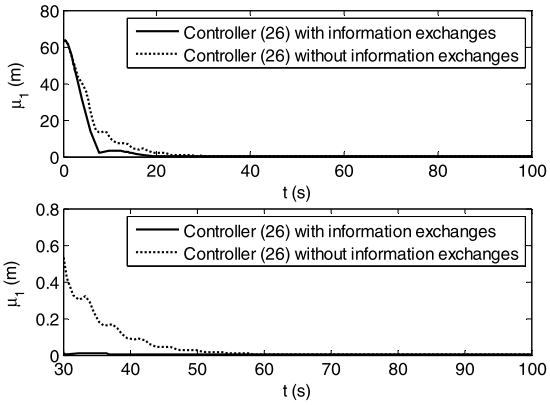

FIGURE 10. Comparision of the formation tracking performance.

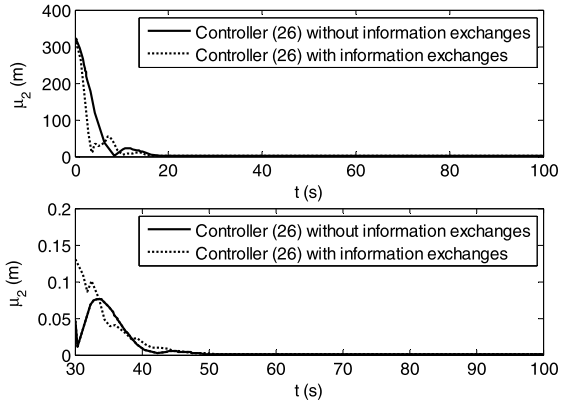

FIGURE 11. Comparision of the formation kepping performance.

the formation tracking error μ_1 and formation keeping error μ_2. It shows that μ_1 and μ_2 can also converge to zero, which implies the favorable formation-tracking and formation-keep performance. The responses of the actual control force $\boldsymbol{F}_i$ are shown in Fig. 7. The developed controllers are clearly able to satisfy the input saturation constraint, while all the components of $\boldsymbol{F}_i$ are not beyond the maximum values of the given bound. Therefore the simulation results demonstrate the validation of the presented controller (20) with actuator saturations.

C. THE SIMULATION RESULTS OF CONTROLLER (26)

The simulation results of the controller (26) are given in Fig. 8-Fig. 11. The position tracking errors of the UAVs are given in Fig. 8, which shows that the position tracking errors decay quickly as the time goes on. From Fig. 9, the velocity errors of the UAVs also converge to zero as the time goes on. So the purpose of tracking the desired trajectory and maintaining the desired configuration is attained. Fig. 10 shows the formation-keeping performance of controller (26) with and without information exchanges (i.e. $c_{ij} = 0$). It is observed that the formation-keeping error μ_1 can both converge to zero finally, and the controller (26) with information exchanges has the advantages of faster convergence velocity and higher tracking precision. The formation keeping error μ_2 with and without information exchanges is presented in Fig. 11, which shows that the controller (26) with information exchanges has faster convergence velocity and equal level tracking precision. In summary, the controller (26) with information exchanges has the better control performance. These simulations verify the feasibility of the developed control algorithms solidly.

V. CONCLUSION

The adaptive backepping control schemes of UAV formation in presence of input saturation and actuator fault constraints are studied. An adaptive backstepping controller with an appropriate command filter is proposed to solve the problem of input saturation and model uncertainty. Then, a robust fault tolerant backstepping controller is introduced to overcome external disturbance, actuator fault and model uncertainty. The stability of the system with the proposed controllers is assured by choosing a reasonable Lyapunov function. It is found that the presented control algorithms enable a fleet of UAVs to form the desired formation if the interaction graph is undirected. The simulation results validate the favorable performance of the developed control methods. It indicates

that the control algorithm with information exchanges has the better control performance. Also, several other topics including collision avoidance and time delay need to be further investigated. These issues will be the subject of the future works.

REFERENCES

[1] W. Lin, "Distributed UAV formation control using differential game approach," *Aerosp. Sci. Technol.*, vol. 35, no. 1, pp. 54–62, 2014.

[2] X. Dong, B. Yu, Z. Shi, and Y. Zhong, "Time-varying formation control for unmanned aerial vehicles: Theories and applications," *IEEE Trans. Control Syst. Technol.*, vol. 23, no. 1, pp. 340–348, Jan. 2015.

[3] H. X. Qiu and H. B. Duan, "Multiple UAV distributed close formation control based on in-flight leadership hierarchies of pigeon flocks," *Aerosp. Sci. Technol.*, vol. 70, pp. 471–486, Nov. 2017.

[4] Q. Ali and S. Montenegro, "Explicit model following distributed control scheme for formation flying of mini UAVs," *IEEE Access*, vol. 4, pp. 397–406, 2016.

[5] Z. Yu, Y. Qu, and Y. Zhang, "Distributed fault-tolerant cooperative control for multi-UAVs under actuator fault and input saturation," *IEEE Trans. Control Syst. Technol.*, to be published.

[6] C. Yuan, Y. Zhang, and Z. Liu, "A survey on technologies for automatic forest fire monitoring, detection, and fighting using unmanned aerial vehicles and remote sensing techniques," *Can. J. Forest Res.*, vol. 45, no. 7, pp. 783–792, 2015.

[7] Z. Yu, Y. Qu, and Y. Zhang, "Safe control of trailing UAV in close formation flight against actuator fault and wake vortex effect," *Aerosp. Sci. Technol.*, vol. 77, pp. 189–205, Jun. 2018.

[8] D. P. Scharf, F. Y. Hadaegh, and S. R. Ploen, "A survey of spacecraft formation flying guidance and control. Part II: Control," in *Proc. Amer. Control Conf.*, Jun./Jul. 2004, pp. 2976–2985.

[9] J. Lavaei, A. Momeni, and A. G. Aghdam, "A model predictive decentralized control scheme with reduced communication requirement for spacecraft formation," *IEEE Trans. Control Syst. Technol.*, vol. 16, no. 2, pp. 268–278, Mar. 2008.

[10] P. Yao, H. Wang, and H. Ji, "Multi-UAVs tracking target in urban environment by model predictive control and improved grey wolf optimizer," *Aerosp. Sci. Technol.*, vol. 55, pp. 131–143, Aug. 2016.

[11] C. Kownacki and L. Ambroziak, "Local and asymmetrical potential field approach to leader tracking problem in rigid formations of fixed-wing UAVs," *Aerosp. Sci. Technol.*, vol. 68, pp. 465–474, Sep. 2017.

[12] L. He, P. Bai, X. Liang, J. Zhang, and W. Wang, "Feedback formation control of UAV swarm with multiple implicit leaders," *Aerosp. Sci. Technol.*, vol. 72, pp. 327–334, Jan. 2018.

[13] J. Zhang, J. Yan, and P. Zhang, "Fixed-wing UAV formation control design with collision avoidance based on an improved artificial potential field," *IEEE Access*, vol. 6, pp. 78342–78351, 2018.

[14] J. Hu, X. Sun, S. Liu, and L. He, "Adaptive finite-time formation tracking control for multiple nonholonomic UAV system with uncertainties and quantized input," *Int. J. Adapt. Control Signal Process.*, vol. 33, no. 1, pp. 114–129, 2019.

[15] K. Lu, Y. Xia, M. Fu, and C. Yu, "Adaptive finite-time attitude stabilization for rigid spacecraft with actuator faults and saturation constraints," *Int. J. Robust Nonlinear Control*, vol. 26, no. 1, pp. 28–46, 2016.

[16] J. A. Farrell, M. Polycarpou, M. Sharma, and W. Dong, "Command filtered backstepping," *IEEE Trans. Autom. Control*, vol. 54, no. 6, pp. 1391–1395, Jun. 2009.

[17] J. Farrell, M. Sharma, and M. Polycarpou, "Backstepping-based flight control with adaptive function approximation," *J. Guid. Control Dyn.*, vol. 28, no. 6, pp. 1089–1102, 2005.

[18] L. Sonneveldt, Q. P. Chu, and J. A. Mulder, "Nonlinear flight control design using constrained adaptive backstepping," *J. Guid., Control, Dyn.*, vol. 30, no. 2, pp. 322–336, 2007.

[19] M. Li, W. Jing, M. Macdonald, and C. R. Mcinnes, "Adaptive backstepping control for optimal descent with embedded autonomy," *Aerosp. Sci. Technol.*, vol. 15, no. 7, pp. 589–594, 2011.

[20] Z. Zheng and S. Song, "Autonomous attitude coordinated control for spacecraft formation with input constraint, model uncertainties, and external disturbances," *Chin. J. Aeronaut.*, vol. 27, no. 3, pp. 602–612, 2014.

[21] G. Cui, S. Xu, F. L. Lewis, B. Zhang, and Q. Ma, "Distributed consensus tracking for non-linear multi-agent systems with input saturation: A command filtered backstepping approach," *IET Control Theory Appl.*, vol. 10, no. 5, pp. 509–516, 2016.

[22] Q. Zhang and H. T. Liu, "UDE-based robust command filtered backstepping control for close formation flight," *IEEE Trans. Ind. Electron.*, vol. 65, no. 11, pp. 8818–8827, Nov. 2018.

[23] Z. Gao, B. Jiang, P. Shi, M. Qian, and J. Lin, "Active fault tolerant control design for reusable launch vehicle using adaptive sliding mode technique," *J. Franklin Inst.*, vol. 349, no. 4, pp. 1543–1560, May. 2012.

[24] P. Li, X. Yu, X. Peng, Z. Zheng, and Y. Zhang, "Fault-tolerant cooperative control for multiple UAVs based on sliding mode techniques," *Sci. China Inf. Sci.*, vol. 60, no. 7, 2017, Art. no. 070204.

[25] Z. X. Liu, X. Yu, C. Yuan, and Y. M. Zhang, "Leader-follower formation control of unmanned aerial vehicles with fault tolerant and collision avoidance capabilities," in *Proc. Int. Conf. Unmanned Aircr. Syst. (ICUAS)*, Jun. 2015, pp. 1025–1030.

[26] X. Yu, Z. Liu, and Y. M. Zhang, "Fault-tolerant formation control of multiple UAVs in the presence of actuator faults," *Int. J. Robust Nonlinear Control*, vol. 26, no. 12, pp. 2668–2685, Aug. 2016.

[27] X. Yu, P. Li, and Y. Zhang, "Fault-tolerant control design against actuator faults with application to UAV formation flight," in *Proc. Chin. Control Conf.*, Jul. 2017, pp. 1768–1934.

[28] W. Ren, "Distributed attitude alignment in spacecraft formation flying," *Int. J. Adapt. Control Signal Process.*, vol. 21, nos. 2–3, pp. 95–113, 2007.

[29] H. Khalil, *Nonlinear Systems*. 3rd ed. New Jersey, NJ, USA: Prentice-Hall, 2002.

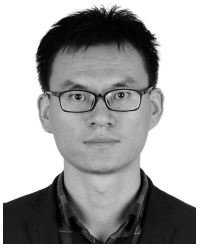

ZHONG ZHENG received the Ph.D. degree from the Harbin Institute of Technology, in 2014. He is currently a Lecturer with the College of Electrical Engineering and Control Science, Nanjing Tech University. His main research interests include spacecraft formation control and nonlinear control.

MOSHU QIAN is currently an Associate Professor with Nanjing Tech University. Her research interests include stability analysis and fault tolerant controller design of the interconnected systems.

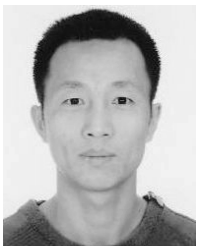

PENG LI received the Ph.D. degree in control science and engineering from the Harbin Institute of Technology, in 2010. He is currently an Associate Professor with the School of Information and Engineering, Xiangtan University. His main research interests include robot guidance, location, and formation control.

HUI YI received the B.E. and Ph.D. degrees from the College of Automation Engineering, Nanjing University of Aeronautics and Astronautics, in 2005 and 2012, respectively. He is currently an Associate Professor with the College of Electrical Engineering and Control Science, Nanjing Tech University. His research interests include fault diagnosis, health monitoring, and artificial intelligence.